© *A. E. Korinenko*[1]*, *V. V. Malinovsky*[1], *V. A. Dulov*[1], *V. N. Kudryavtsev*[1,2], 2022
© Translation from Russian: *E. S. Kochetkova*, 2022

[1]Marine Hydrophysical Institute, Russian Academy of Sciences, 299011, Kapitanskaya Str., 2, Sevastopol, Russia
[2]Russian State Hydrometeorological University, 195196, Malookhtinsky Pr., 98, St. Petersburg, Russia
*E-mail: korinenko.alex@mhi-ras.ru

ESTIMATION OF THE "WHITECAP" LIFETIME OF BREAKING WAVE

Received 04.09.2021, revised 28.12.2021, accepted 10.01.2022

Abstract

The paper presents the results of a study of the lifetime of wind-wave breaking ("whitecaps") and the spatial distribution of the moments of wave-breaking initiation along the profile of a long surface wave. The results obtained during the specialized experiments from an oceanographic platform in the Black Sea are given. The registration of the whitecaps was carried out based on the video recordings of the sea surface. The surface waves' characteristics were measured and the meteorological information was recorded simultaneously with the video recordings.

It is shown that the distribution of the whitecaps' lifetime is well described by an exponential law. It was found that the ratio of the lifetime of an individual whitecap to the period of the breaking wave is 0.3. The distributions of the above-mentioned ratio are similar for different wind and wave conditions. It is indicated that the generation of whitecaps occurs mainly in the region of the crest of a long wave with a shift to its front slope on average by 9.6 of the phase of the long wave. The whitecap having arisen at the leading edge shifts to the trailing edge of the long wave during its lifetime, so that the phase difference between the breaking initiation and the maximum of the surface fraction covered by the whitecaps equals 21.6.

Keywords: wind wave breaking, whitecap lifetime, field studies, initial moment of wind wave breaking, modulation of short wave breaking by long waves

© *А. Е. Кориненко*[1]*, *В. В. Малиновский*[1], *В. А. Дулов*[1], *В. Н. Кудрявцев*[1,2], 2022
© Перевод с русского: *Е. С. Кочеткова*, 2022

[1]Морской гидрофизический институт РАН, 299011, Капитанская ул., 2, г. Севастополь, Россия
[2]Российский государственный гидрометеорологический университет, 195196, Малоохтинский пр., д. 98, г. Санкт-Петербург, Россия
*E-mail: korinenko.alex@mhi-ras.ru

ОЦЕНКА ВРЕМЕНИ ЖИЗНИ «БАРАШКА» ОБРУШИВАЮЩЕЙСЯ ВОЛНЫ

Статья поступила в редакцию 04.09.2021, после доработки 28.12.2021, принята в печать 10.01.2022

Аннотация

Представлены результаты исследования времени жизни обрушений ветровых волн (барашков) и пространственного распределения моментов зарождения обрушений по профилю длинной поверхностной волны, полученные в ходе специализированных экспериментов с океанографической платформы в Черном море. Регистрация барашков осуществлялась по видеозаписям морской поверхности. Одновременно с видеозаписями измерялись характеристики поверхностного волнения, а также регистрировалась метеорологическая информация.

Показано, что распределение времени жизни барашка хорошо описывается экспоненциальным законом. Установлено, что отношение времени жизни индивидуального барашка к периоду обрушивающейся волны равно 0,3, а распределения этого отношения подобны для различных ветровых и волновых условий. Показано, что зарождение барашков происходит преимущественно в районе гребня длинной волны со смещением на ее передний склон в среднем на 9,6° фазы длинной волны. Возникнув на переднем фронте, барашек за время жизни смещается на задний фронт длинной волны, так что разность фаз между зарождением обрушения и максимумом доли поверхности, занятой барашками, составляет 21,6°.

Ссылка для цитирования: *Кориненко А.Е.*, *Малиновский В.В.*, *Дулов В.А.*, *Кудрявцев В.Н.* Оценка времени жизни «барашка» обрушивающейся волны // Фундаментальная и прикладная гидрофизика. 2022. Т. 15, № 1. С. 61–72.
doi: 10.48612/fpg/5g5t-4mzd-94ab
For citation: *Korinenko A.E.*, *Malinovsky V.V.*, *Dulov V.A.*, *Kudryavtsev V.N.* Estimation of the "Whitecap" Lifetime of Breaking Wave. *Fundamental and Applied Hydrophysics*. 2022, 15, 1, 61–72. doi: 10.48612/fpg/5g5t-4mzd-94ab

Ключевые слова: обрушения ветровых волн, время жизни барашка, натурные исследования, начальный момент обрушения ветровой волны, модуляция обрушений коротких волн длинными волнами

1. Introduction

Wind wave breaking plays an important role in the sea surface processes, including a gas exchange between the ocean and the atmosphere [1], wind-wave energy dissipation [2], turbulence generation in the near-surface layer of the sea [3], sea spray generation [4], and affect the atmospheric boundary layer structure [5, 6]. The breaking intensity is sensitive to surface currents' irregularities associated with various oceanic dynamic processes (internal waves, boundaries of sub- and mesoscale currents, fronts), which is advantageous for remote sensing applications [7–9].

Wave breaking on the sea surface is a complex hydrodynamic phenomenon. A whitecap forms when a breaking wave entrains air into the surface layer of water. The foam area significantly enlarges as it propagates with the wave crest. Over time, a trail of residual foam appears behind the whitecap. According to a nomenclature [10, 11], the whitecap is considered an active phase of wave breaking "phase A" and residual 'plume of foam' is characterized by clouds of emerging air bubbles, as a passive "phase B" [10, 11]. The spatiotemporal stochastic dynamics and electrodynamics of these phases are fundamentally different [12]. Hence, the role of these phases in physical sea surface phenomena also differs, and, accordingly, the importance of their study for various specific applications. For example: "phase B" [12] is the most important in the phenomena of gas exchange and intrinsic microwave radiation of the sea surface, while for the visualization of the wave energy dissipation [2] and the formation of a radar signal, the whitecaps — "phase A" [13, 14] are of primary interest. Due to the optical registration of the sea surface at observation angles of about 45 degrees, in this study, we focus on the temporal evolution of the whitecaps that occur when a gravity wind-wave breaks.

As shown by the studies [15, 16], the characteristic lifetime of wave breaking in "phase B" lasts seconds, and the duration of "phase A" is tenths of a second. Therefore, in natural experiments, it is difficult to determine the lifetime of a whitecap, and the results of scarce studies [17–20] are contradictory. Depending on the wind-wave conditions, the average value of the breakage lifetime $\overline{\tau}$ according to radar measurements in the range of electromagnetic waves of 3 cm varies from 0.8s to 3s [19]. According to acoustic measurements, it lasts 1.2s to 1.8s. At the same time, the analysis of the $\overline{\tau}$ distribution obtained in the Black Sea in the area of the Stationary Oceanographic Platform in [20] shows that $0.3 \le \overline{\tau} \le 0.8$ s. When studying the average lifetime of a whitecap, the ratio between $\overline{\tau}$ and the average period of a breaking wave $\overline{T}$ is of interest. According to [17] $\overline{\tau}$ is 45–65 % of $\overline{T}$. A study [21] showed that for single breaking, the ratio of τ to the wave breaking period is within 0.3–0.5. As a result of radar measurements [19], the value $\tau/T \cong 0.8$. The listed discrepancies point to the necessity of further studies of the whitecaps' lifetime, one of the main physical characteristics of wave breaking.

Under natural conditions, wind-wave breaking occurs in the presence of long waves such as spectral peak wind waves and/or swell waves. Long wind waves rarely break [22] but cause modulation of shorter waves breaking [23–25].

As a result, the whitecaps are concentrated in the vicinity of the long wave crest. At the same time, the maxima of breakage-covered areas Q are shifted towards the rear slope of a modulating wave [25]. It seems to contradict the theoretical concepts, according to which the maximum amplitude of short waves should be on the front slope close to the long wave crest [26, 27]. The observed discrepancy in Q localization is analyzed in [25], where the shift of the Q maximum to the rear slope is explained by the whitecaps' finite lifetime. Whitecaps lag behind the long wave crest due to the difference in the phase velocities of the short breaking waves and the long wave. These findings inspired our interest in detailed estimates of the whitecaps' lifetimes and the starting point of the breaking in the presence of the long waves. If these time points appear to localize in the short waves' amplification regions, theoretically predicted to occur before the long wave crest, the study findings [25] will be expanded significantly.

The aim of this work is to study the statistical characteristics of the breaking lifetimes, their relationship with the period of the breaking wave, and the study of the initial breaking time points distribution on the long wave profile.

2. Field experiment

2.1. General description

Field experiments took place in the autumn of 2015, 2018–2019, from an oceanographic platform in the Black Sea near the village Katsiveli. The station is 0.5 km offshore, at about 30 m water depth. The observations were made during stable wind from the sea and consisted of synchronous video recording of the sea surface, sea surface elevations measurements, and wind speed records (see Fig. 1).

A digital video camera with a recording frequency of 25 frames per second and a resolution of 1920 × × 1080 pixels was used to register the breaking of wind waves. The camera was located at an altitude of 12 m above sea level. The angle between the optical axis of the video camera and the sea surface was set to be 35°–45°. The horizontal viewing angle of the lens was 54°, and the vertical was 32°. The sea surface heights were recorded by a string wave gauge located at the end of an 11 m long boom. Meteorological information was collected by a *Davis 6152EU* multifunctional complex positioned at 23 m above sea level on the mast of an oceanographic platform (see Fig. 1). The measured wind speeds were recalculated as wind speed U at 10 m using air and water temperature and humidity data following the method [28]. The experiments were carried out at wind speeds of 9 m/s— 21m/s. A detailed measurement technique and a description of the instruments are given in [29, 30].

2.2. Whitecaps’ lifetimes

To estimate the lifetimes of whitecaps, we used video data with a frame that covered an area of the sea surface of about 400 m^2. Based on a known recording geometry, the image frame was georeferenced to coordinates on a horizontal plane attributed to a mean sea level. The resolution along the vertical axis varied from 0.01 m to 0.06 m and from 0.01 m to 0.02 m along the horizontal axis.

The algorithm from [31] was used to identify whitecaps on video footage of the sea surface. The algorithm is based on the difference between the modeled foam-free Gaussian brightness distribution I in a video frame

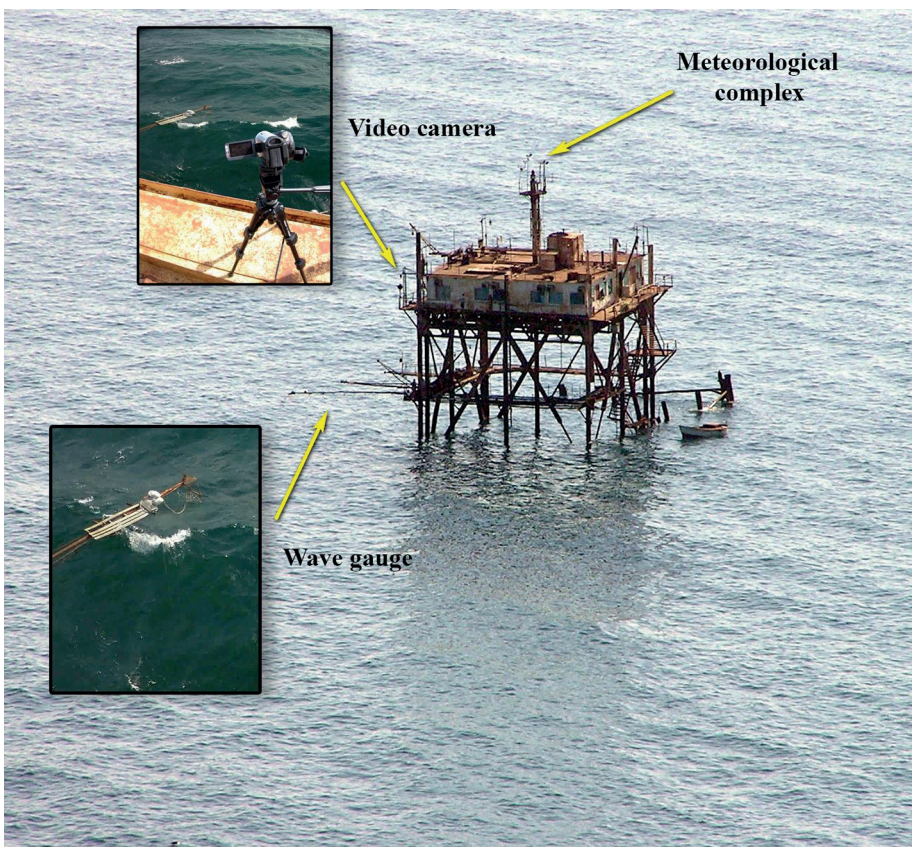

Fig. 1. The instrumentation layout on the oceanographic platform

and the actual brightness distribution in the presence of foam structures. The foam structures distort the "tail" of the normal distribution $p(I)$ at high brightness values. The threshold value is a brightness level I_0 above which distortions $p(I)$ are observed; therefore, foam structures are areas with exceeding brightness I_0. For subsequent analysis, only the active phase of the breaking ("phase A" whitecaps) was distinguished, and the spots of spreading foam remaining after the breaking passage were automatically filtered out using the kinematic properties of the breaking in different phases [31–33].

The main difference in the kinematics of the phases is reflected in the fact that the whitecaps propagate in a horizontal plane at an almost constant velocity, while trajectories of the residual foam structures are chaotic. Figure 2 shows the evolution of a whitecap from the moment of its emergence (see the enlarged inset in Fig. 2, *a*) until its disappearance, after which only a spot of spreading foam remained on the sea surface, visible near the lower boundary of Fig. 2, *e*. The whitecaps and spreading foam appear as bright white formations. The highlighted red pixels were identified by the algorithm [31] as the active phase of the breaking. As the whitecap develops around the red area (the whitecap itself), you can see white pixels corresponding to clouds of pop-up bubbles.

Figure 3 shows the evolution of the area (Fig. 3, *a*) and the movement of the geometric center (X, Y) in more detail in the local coordinate system (Fig. 3, *b*) of the same foam formation. Symbols (•) in Fig. 3*a* correspond sequentially to the frames shown in Fig. 2, *a–e*. Similar examples of the geometric characteristics evolution of whitecaps are illustrated in other studies also (see, for example, Figs. 3 and 4 in [22] and Fig. 3 in [30]). The whitecap temporal evolution, which is moving at a specific speed, is characterized by its area expansion up to a certain maximum. Then the whitecap begins to scatter into spots of residual foam. During this stage, the propagation of the bright region geometric center slows down significantly. Finally, it assumes an oscillatory character of the dominant waves' orbital motions. During the foam structure area decline, "phases A and B" are indistinguishable in the visible range images. However, the physics of the breaking wave phenomenon implies that the bright region of active breaking (whitecap) is rigidly connected with the breaking wave and therefore moves with its phase velocity [34]. Consequently, active phase A should include bright areas moving at a constant speed. The time when such a movement occurs corresponds to the whitecap area growth. When analyzing the statistical characteristics of the active phase of breaking, as a rule, only the stage of the area growth is considered, ignoring foam structures in the stage of its decline (see, for example, [22, 30, 31–33]).

The algorithm [31], using a decision tree based on the kinematic parameters of the foam area, makes it possible to adequately identify the 'phase A' of breaking (see Fig. 2). The time point of the whitecaps' maximum area denoted the breaking time (in Fig. 3, *a*, a vertical line marks this point in time). The period between registration and the whitecap maximum size indicated its lifetime. For this study, we only consider whitecaps that originated and disintegrated within the observed region.

As follows from Fig. 3, *b*, before the breaking, a whitecap propagates steadily with a phase velocity of $c = \sqrt{\dot{X}^2 + \dot{Y}^2}$. We considered this velocity to be equal to the phase velocity of the breaking wave, as proposed by O.M. Phillips [34]. Further, using the dispersion relation of short gravity waves, the periods of carrier waves were computed for each whitecap as $T = 2\pi c/g$, where g is gravity acceleration.

2.3 Initiation of breaking under the influence of long waves

A series of eight specific experiments were carried out in 2018 at wind speeds of 13 m/s-19 m/s [25] to study breaking modulations by long waves. The camera pointed towards the direction of long waves, which always coincided with the direction of the wind. The sea surface section was video recorded at its intersection with the string wave gauge (see Fig. 2). At the same time, the wave recorder was synchronized with the video camera and recorded its signal in parallel with the video sound into a single file. Synchronization accuracy was 1ms. As a result, [25] reported the distribution of the whitecap surface fraction at the long wave profile. The present work answers the question of how the breaking initiation times are distributed at the long wave profile.

In this part of the experiment, special attention was paid to the wave breaking initial stage detection, when the whitecap is just beginning to form. We determined the times of breaking initiation in a square section with a side $L_m = 0.9$ m and centered at the point of intersection with the wave string gauge (see Fig. 2, where the green box shows the section boundaries).

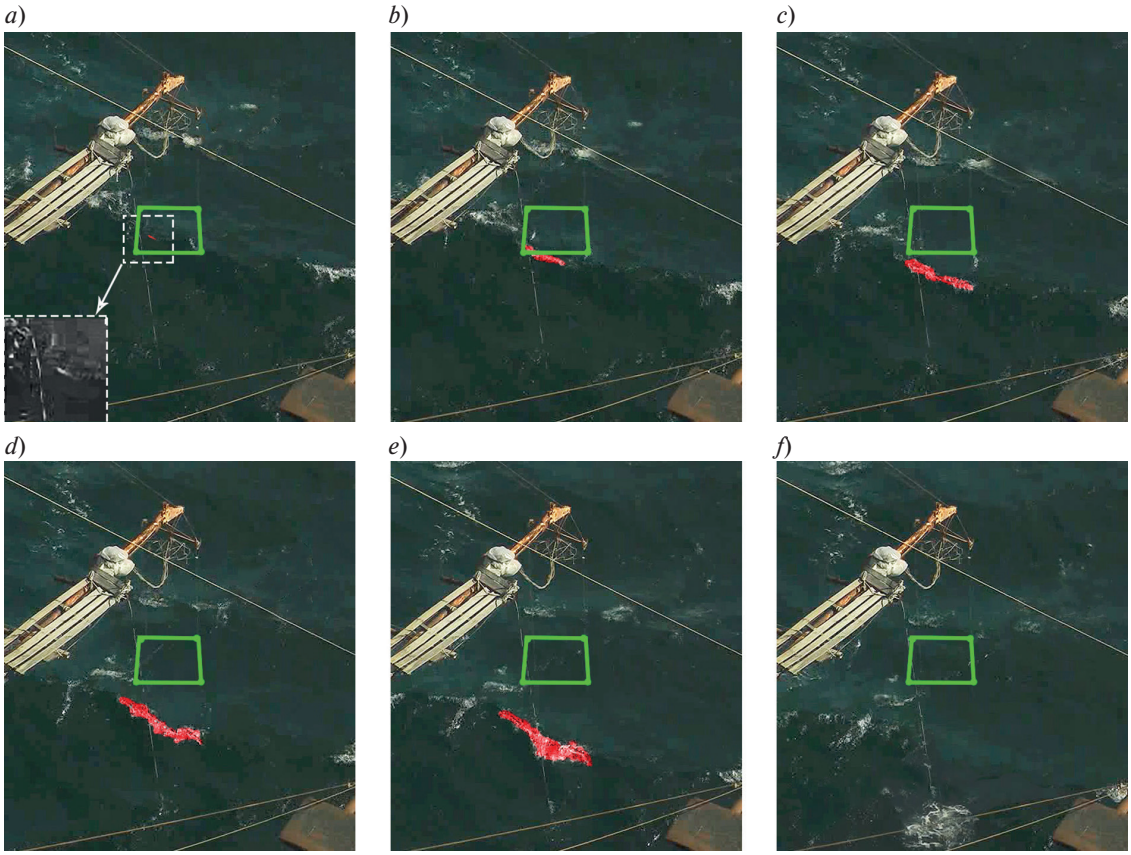

Fig. 2. Evolution of wave breaking: *a* — the moment of whitecap generation; *b*–*e* — movement and growth of the whitecap; *f* — a spot of spreading foam after the disappearance of the whitecap. The active phase of the breaking is highlighted in red according to the applied algorithm [31]. The square area used is shown by green box

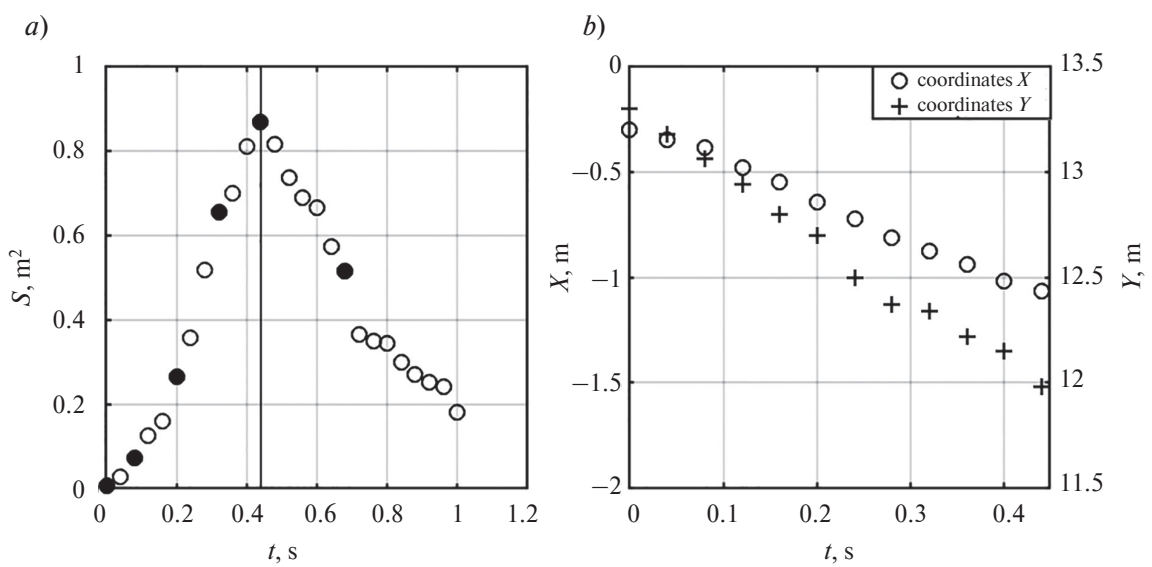

Fig. 3. Changes in the area, *S*, (*a*) and coordinates of the geometric center *X* and *Y*, (*b*) of breaking shown in Fig. 2. The symbols (•) correspond to the video frames shown in Fig. 2. The vertical line indicates the moment of whitecap disappearance

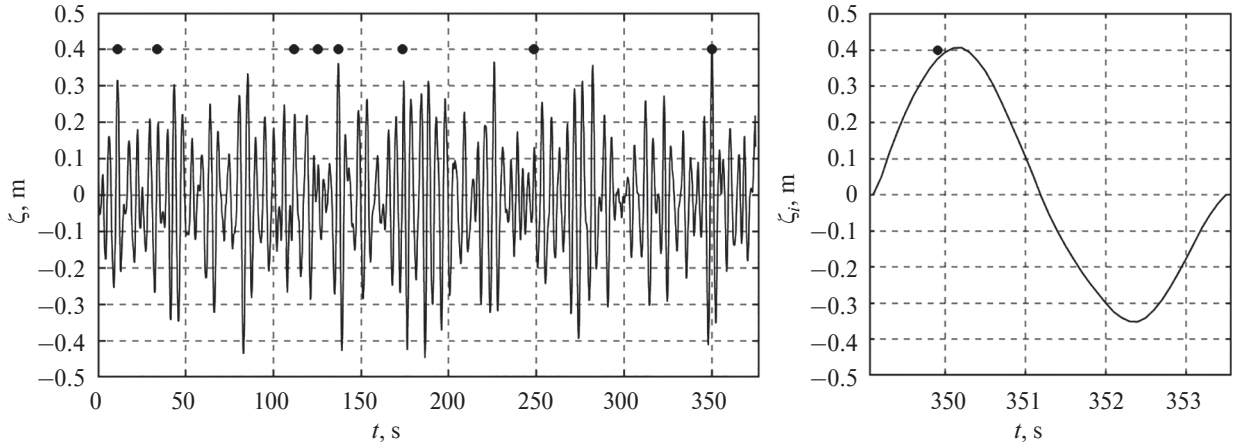

Fig. 4. A record fragment of the sea surface elevations $\zeta(t)$ with the marks (•) at the moments of the beginning of the breaking. An individual breaking event is zoomed on the right panel

Fig. 4 gives an example of the obtained data, the elevations of the sea surface $\zeta(t)$ and the breaking initiation tied to them in time. Individual waves were analyzed (see, for example, [23, 25]) to obtain the long waves' characteristics. The passing of zero by the signal in the "upward" direction $\zeta(t)$ was recorded as an initiation of an individual wave, which existed until the next signal crossing of zero "downward" (see the example in Fig. 4 on the right). The duration of an individual wave was considered its period T_i. Then the phase of the wave at time t is $\Phi = 2\pi(t - t_i)/T_i$, where t_i corresponds to the initiation of the wave. The wavenumber of an individual wave was determined as $K_i = (2\pi/T_i)^2/g$, and multiplied by the wave amplitude to obtain the wave steepness parameter AK.

The resulting database comprises more than 1300 individual waves. Methodology details for this processing, estimation of errors, and a detailed description of the meteorological conditions during these experiments are given in [25].

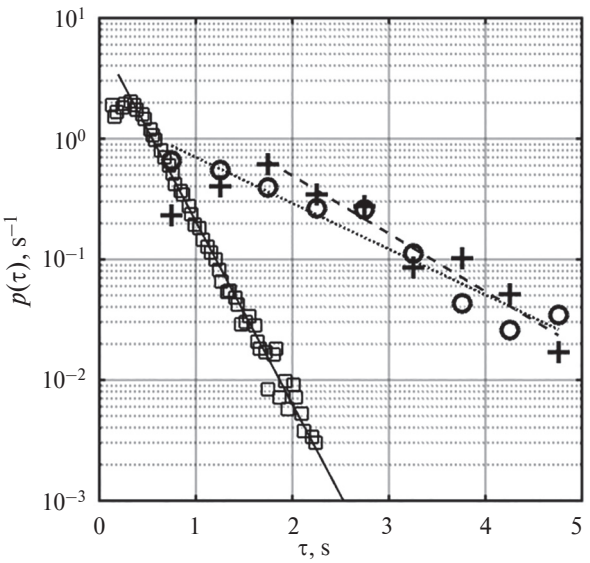

Fig. 5. Probability densities of the breaking lifetime. Symbols (□) are our measurements, (○) and (+) — the data from [17] and [19]. Lines are approximating curves, $p(\tau) = p \cdot \exp(-q \cdot \tau)$

3. Results

3.1. Breaking lifetime statistics

Fig 5 shows the probability density $p(\tau)$, of the entire dataset and the good exponential fit $p(\tau) = 6.88 \cdot \cdot \exp(-3.49 \cdot \tau)$, plotted in solid line. The average value for all data is $\overline{\tau} = 0,46$ s. The exponential form of the distribution agrees with the results presented in [19], where the average lifetime was 0.4 s.

The mentioned average values of the breaking lifetimes $\overline{\tau}$ and the distributions $p(\tau)$, obtained from acoustic and radar measurements presented in [17] and [19], respectively, are significantly larger than those obtained from our experiment. The values $\overline{\tau}$ discrepancy could be due to the difference in methods. In our experiments using video camera and video frame processing technique minimum duration of $\tau_{min} = 0.12$ s, while [17] and [19] τ_{min} minimum is 0.5 s. The small-scale breakers are observed in radar images, as noted in [19]. However, most of them are below τ measurement threshold, and a significant number of the breakers remain ignored. The histogram τ shows a maximum at τ

= 1.75 s with a decrease of the registered events number to the left of the peak (see Fig. 3 in [19]). The acoustic measurement method [17] gives $\tau > 2$ at 45 % of breakers. Thus, high $\bar{\tau}$ values obtained by acoustic and radar methods can be associated with registration of both the breaks with a minimum value of $\tau_{min} \sim 0.5–0.7$ and the "phase B". Both lead to an overestimation of $\bar{\tau}$. It is important to note that given in [17] and [19], the breaking lifetimes were measured in the open ocean with characteristic wave periods of 5–7 s and included swell.

Histograms $H(\tau)$, in [19] include both radar and acoustic data (provided by the authors of [17]). Using the values of both histograms, we calculated the probability density of τ, corresponding to these measurements, marked in Fig. 5 with symbols (◊) and (○). Just as in our case, the $p(\tau)$ curves are satisfactorily fitted by the exponential law $p(\tau) = p \cdot \exp(-q \cdot \tau)$, where the coefficients p are 1.51 and 0.52, the q values are 1.1 and 0.9 for the [19] and [17] data, respectively. Here, when calculating $p(\tau)$ for the data, the statistically infrequent values of $H(\tau)$, to the left of the maximum, were ignored (see the results' analysis in [19]).

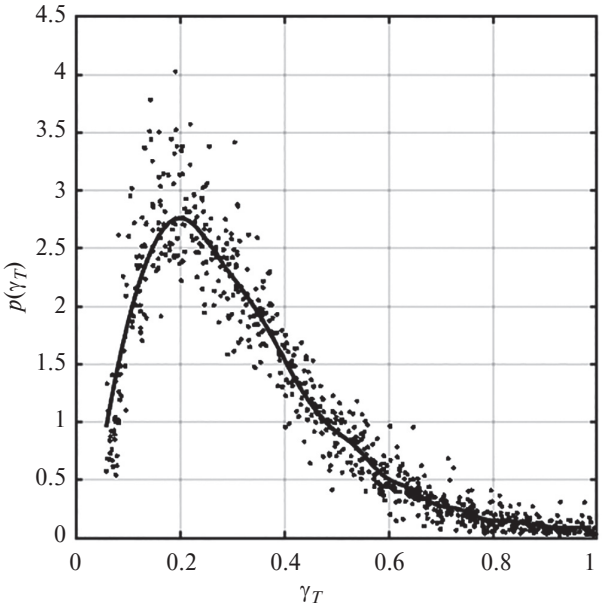

Fig. 6. Distributions of the ratios of breaking lifetime to the period of the breaking wave γ_T for all measurements, the solid line is the result of averaging

Figure 6 shows the distributions of the ratio of the whitecap lifetime to the period of breaking waves $\gamma_T = \tau/T$ for individual breaking events. The distributions for sixty-four samples collected at various wind speeds are shown by dots. The solid line shows the averaged distribution γ_T. The standard deviation from average is $\sqrt{\overline{(\gamma_T)^2}} = 0.13$, confirming that the distributions γ_T for different wind speeds have similar shapes, the estimate of which is represented by the averaged distribution. The distribution maximum is observed at $\gamma_T = 0.2$. The average value of the ratio of the whitecap lifetime to the period of the breaking wave is $\overline{\gamma_T} = 0.3$. The values of γ_T are in the range of 0.1–0.41 with a probability of 75 % and in the range of 0.1–0.56 with a probability of 90 %.

3.2. Distribution of breaking initiation events at the long wave profile

Figure 7 shows the distributions of breaking initiation events at the long wave profile for all series of measurements. Each event is characterized by a phase of a long wave (see section 2.3), so unnormalized distributions are obtained by constructing histograms for these phases $N(\Phi)$. Also, Fig. 7 shows the averaged dimensionless profiles of long waves $\zeta(\Phi) = \overline{K_i \zeta_i(\Phi)}$, where the averaging is performed over all individual waves in the sampling at a fixed phase.

The main feature of $N(\Phi)$ is that the points of whitecap origin are concentrated about the wave crest and occur much less frequently in the wave trough. While the average profile of the long wave is sinusoidal, the average profile of the number of breaks has a pronounced asymmetric appearance. To determine the phase shift Φ_1 between realizations z and N we present the obtained profiles of N in the form of a truncated Fourier expansion $N = \bar{N} + N_1 \sin(\Phi - \Phi_1) + \ldots$. Positive Φ_1 denotes the shift of maximum N to the back slope of the wave. Figure 8 shows the dependences of Φ_1 on the average slope of the long wave $\overline{KA}$ and wind speed U together with the proportion of the surface Q, occupied by whitecaps, which were obtained in [25]. Fig. 8 shows that Φ_1 is practically independent of $\overline{KA}$ and U in the studied range of these values. The phase shift Φ_1 of Q are shifted to the backslope for 11.6° average, while the timepoints of breaking initiation are shifted to the forward slope for –9.6° on average.

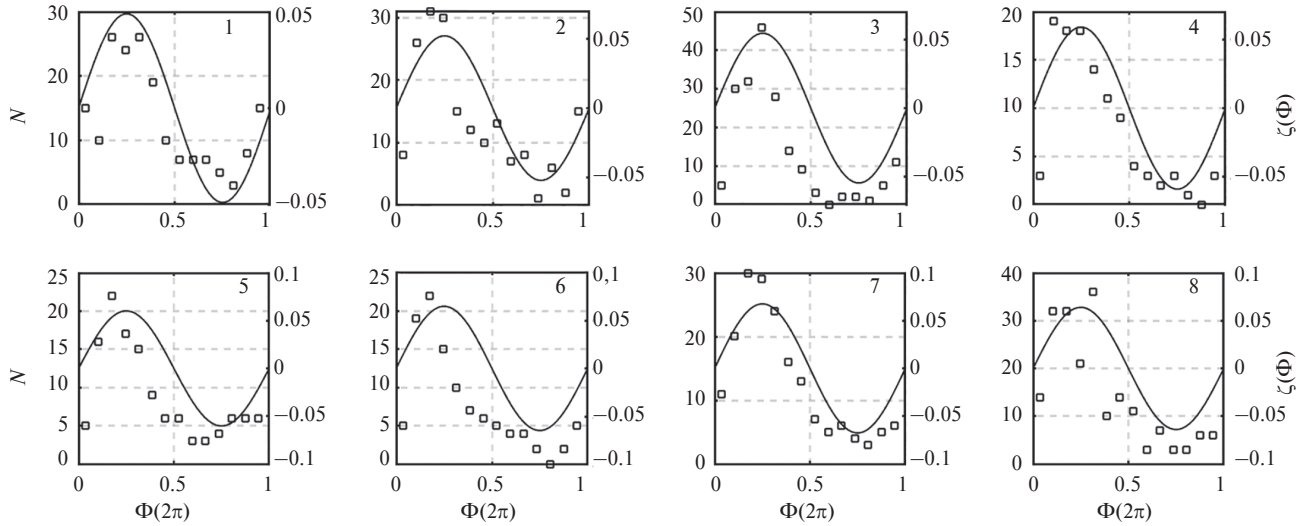

Fig. 7. Unnormalized distribution of events of the breaking beginning N (symbols) along the long wave profile for all series of measurements. Solid lines are the averaged profiles of long waves $\zeta(\Phi)$

This difference in the phase shifts of Q and N is associated with the finite whitecap lifetime. According to the physical model [25], breakings are formed mainly on the crest of the dominant wave. The whitecap, moving with the breaking short wave's phase velocity c during lifetime τ, will lag behind the crest of the long wave moving with its phase velocity C. Then the estimation of the phase shift $\Delta\Phi$ between N and Q is determined by the whitecap displacement relative to the long wave during the lifetime τ: $\Delta\Phi = K(C - c) \cdot \tau$ [25], where K is the wavenumber of the long wave. If we characterize long waves by their average phase velocity $C = 8.2$m/s (calculated by averaging over all individual long waves), and short breaking waves by average phase velocity $c = 2.5$ m/s, then, considering the previously obtained estimate $\tau \approx 0.3T$, we arrive at the phase shift value $\Delta\Phi = 24°$, which agrees well with the experiment.

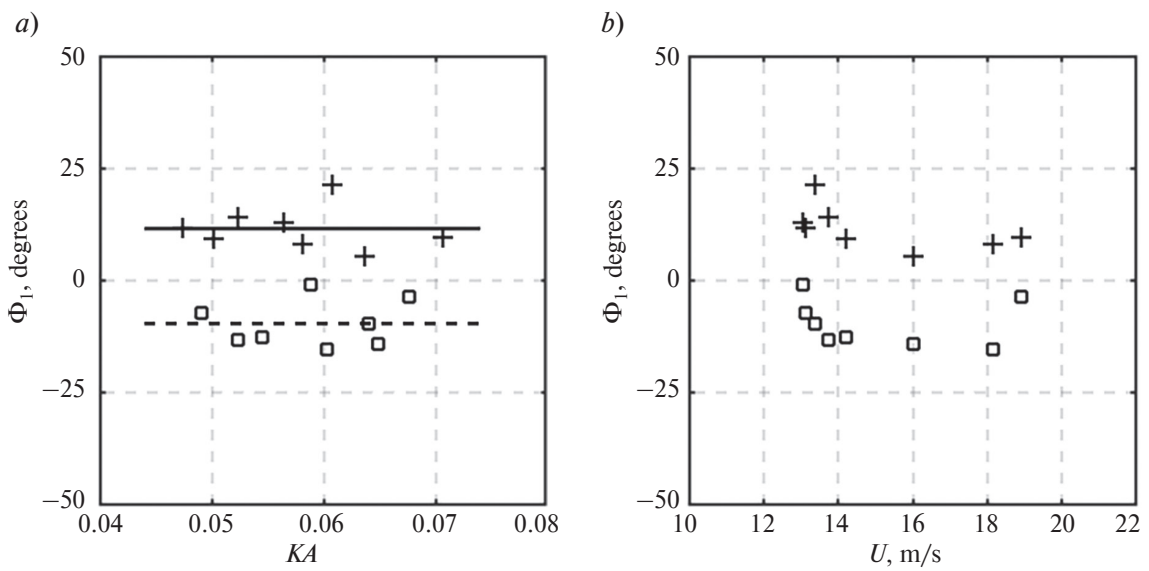

Fig. 8. Dependence of the phase shift Φ_1: *a* — on the wave steepness; *b* — on the wind speed. Symbols (□) represent the present paper data, symbols (+) show the results of [25]. The levels of the solid lines correspond to the mean values –9,6° for our data and 11,6° for the data of [25]

4. Conclusions

This paper presents the results of two experiments carried out on the Stationary Oceanographic Platform in the Black Sea using a video camera and a string wave recorder at wind speeds from 9 to 21 m/s.

The breaking lifetime (duration) τ is well described by an exponential law. The probability density τ form agrees with the results of [17, 19, 20]. The average breaking lifetime for all records is 0.46s, which is significantly shorter than the values obtained from acoustic (1.3–1.7 s [17]) and radar (0.7–3 s [19]) measurements.

The probability densities of the ratios of the duration of individual breakings to the period of breaking waves, γ_T, obtained for 64 series of measurements under various hydrometeorological conditions, coincide. The distributions γ_T have a maximum at $\gamma_T = 0.2$. With a probability of 75 % the values of γ_T are in the range of 0.1–0.41 and with a probability of 90 % lie in the range between 0.1 and 0.56. The average value of the ratio of the whitecap lifetimes to the period of the corresponding breaking waves is 0.3, which coincides with the values $0.3 \le \overline{\gamma_T} \le 0.5$, given in [21], but lower than the estimate $\tau/T \cong 0.8$, obtained in [19].

The whitecaps originate mainly near the long wave crest and shifted to its front slope by 9.6° of the long wave phase. The fact that the initial breaking moments are concentrated on the leading slope of the modulating wave corresponds to the theoretical conclusions [26, 27]. At the same time, as reported in [25], the maximum fraction of the surface covered by whitecaps is shifted by 11.6° of the long wave phase to the back slope relative to its crest. Therefore, a whitecap originates on the front slope, and during its lifetime, it shifts to the long wave back slope by ~21° on average, which confirms the conclusions of [25].

5. Funding

The work was funded by the grant of the Russian Science Foundation No. 21-17-00236, https://rscf.ru/project/21-17-00236/, using archival data collected in the course of the state assignments 0555-2021-0004 and 0763-2020-0005.

References

1. *Zappa C.J.*, *McGillis W.R.*, *Raymond P.A.*, *Edson J.B.*, *Hintsa E.J.*, *Zemmelink H.J.*, *Dacey J.W.H.*, *Ho D.T.* Environmental turbulent mixing controls on air-water gas exchange in marine and aquatic systems. *Journal of Geophysical Research Letters*. 2007, 34, 10. doi: 10.1029/2006GL028790
2. *Thorpe S.A.* Energy loss by breaking waves. *Journal of Physical Oceanography*. 1993, 23, 11, 2498–2502. doi: 10.1175/1520-0485(1993)023<2498: ELBBW>2.0.CO;2
3. *Kudryavtsev V.N.*, *Shrira V.*, *Dulov V.A.*, *Malinovsky V.V.* On the vertical structure of wind-driven sea currents. *Journal of Physical Oceanography*. 2008, 38, 10, 2121–2144. doi: 10.1175/2008JPO3883.1
4. *Troitskaya Y.*, *Kandaurov A.*, *Ermakova O.*, *Kozlov D.*, *Sergeev D.*, *Zilitinkevich S.* Bag-breakup fragmentation as the dominant mechanism of sea-spray production in high winds. *Scientific Reports*. 2017, 7, 1614. doi: 10.1038/s41598-017-01673-9
5. *Kudryavtsev V.*, *Chapron B.* On growth rate of wind waves: impact of short-scale breaking modulations. *Journal of Physical Oceanography*. 2016, 46, 1, 349–360. doi: 10.1175/JPO-D-14-0216.1
6. *Troitskaya Y.*, *Sergeev D.*, *Kandaurov A.*, *Vdovin M.*, *Zilitinkevich S.* The effect of foam on waves and the aerodynamic roughness of the water surface at high winds. *Journal of Physical Oceanography*. 2019, 49. doi: 10.1175/JPO-D-18-0168.1
7. *Thorpe S.A.*, *Belloul M.B.*, *Hall A.J.* Internal waves and whitecaps. *Nature*. 1987, 330, 740–742. doi: 10.1038/330740a0
8. *Dulov V.A.*, *Kudryavtsev V.N.*, *Sherbak O.G.*, *Grodsky S.A.* Observations of wind wave breaking in the gulf stream frontal zone. *The Global Atmosphere and Ocean System*. 1998, 6, 3, 209–242.
9. *Kubryakov A.A.*, *Kudryavtsev V.N.*, *Stanichny S.V.* Application of Landsat imagery for the investigation of wave breaking. *Remote Sensing of Environment*. 2021, 253, 112144. doi: 10.1016/j.rse.2020.112144
10. *Bondur V.G.*, *Sharkov E.A.* Statistical characteristics of foam formations on a disturbed sea-surface. *Okeanologiya*. 1982, 22, 3, 372–378 (in Russian).
11. *Monahan E.C.*, *Woolf D.K.* Comments on "Variations of whitecap coverage with wind stress and water temperature". *Journal of Physical Oceanography*. 1989, 19, 5, 706–709. doi: 10.1175/1520–0485(1989)019<0706: COOWCW>2.0.CO;2
12. *Sharkov E.A.* Breaking ocean waves: geometry, structure and remote sensing. *Berlin*; *Heidelberg*; *N.Y.*, *Springer/PRAXIS*, 2007. 278 p.

13. *Phillips O.M.* Radar returns from the sea surface-Bragg scattering and breaking waves. *Journal of Physical Oceanography*. 1988, 18, 8, 1065–1074. doi: 10.1175/1520–0485(1988)018<1065: RRFTSS>2.0.CO;2
14. *Kudryavtsev V.N.*, *Hauser D.*, *Caudal G.*, *Chapron B.* A semiempirical model of the normalized radar cross-section of the sea surface 1. Background model. *Journal of Geophysical Research*. 2003, 108, C3. doi: 10.1029/2001JC001003
15. *Sharkov E.A.* Experimental studies of the lifetime of the dispersed phase of a breaking gravitational wave. *Izvestiya AN USSR Fizika Atmosfery i Okeana*. 1994, 30, 6, 844–847 (in Russian).
16. *Callaghan A.H.*, *Deane G.B.*, *Stokes M.D.*, *Ward B.* Observed variation in the decay time of oceanic whitecap foam. *Journal of Geophysical Research*. 2012, 117, C9. doi: 10.1029/2012JC008147
17. *Ding L.*, *Farmer D.M.* Observation of breaking surface wave statistics. *Journal of Physical Oceanography*. 1994, 24, 6, 1368–1387. doi: 10.1175/1520-0485(1994)024<1368: OOBSWS>2.0.CO;2
18. *Bortkovskii R.S.*, *Novak V.A.* Statistical dependences of sea state characteristics on water temperature and wind-wave age. *Journal of Marine Systems*. 1993, 4, 2–3, 161–169. doi: 10.1016/0924-7963(93)90006-8
19. *Phillips O.M.*, *Posner F.L.*, *Hansen J.P.* High range resolution radar measurements of the speed distribution of breaking events in wind-generated ocean waves: Surface impulse and wave energy dissipation rates. *Journal of Physical Oceanography*. 2001, 31, 2, 450–460. doi: 10.1175/1520-0485(2001)031<0450: HRRRMO>2.0.CO;2
20. *Mironov A.S.*, *Dulov V.A.* Statistical characteristics of events and energy dissipation during wavebreaking. *Sbornik Nauchnykh Trudov. NAN Ukrainy*, *MGI*, *Sevastopol*. 2008, 16, 97–115 (in Russian).
21. *Thorpe S.A.*, *Hall A.J.* The characteristics of breaking waves, bubble clouds, and near-surface currents observed using side-scan sonar. *Continental Shelf Research*. 1983, 1, 4, 353–384. doi: 10.1016/0278-4343(83)90003-1
22. *Pivaev P.D.*, *Kudryavtsev V.N.*, *Korinenko A.E.*, *Malinovsky V.V.* Field observations of breaking of dominant surface waves. *Remote Sensing*. 2021, 13, 16, 3321. doi: 10.3390/rs13163321
23. *Dulov V.A.*, *Kudryavtsev V.N.*, *Bol'shakov A.N.* A field study of whitecap coverage and its modulations by energy containing surface waves. *Gas Transfer at the Water Surface*. Geophys. Monogr. 127 / Ed. Donelan M.A., Drennan W.M., Saltzman E.S., Wanninkhof R. *AGU*, *Washington DC*, *USA*, 2002, 187–192. doi: 10.1029/GM127p0187
24. *Yurovsky Y.Y.*, *Kudryavtsev V.N.*, *Chapron B.* Simultaneous radar and video observations of the sea surface in field conditions. *Proceedings of the Electromagnetics Research Symposium — Spring (PIERS). St. Petersburg*, 2017, 2559–2565. doi: 10.1109/PIERS.2017.8262183
25. *Dulov V.A.*, *Korinenko A.E.*, *Kudryavtsev V.N.*, *Malinovsky V.V.* Modulation of wind-wave breaking by long surface waves. *Remote Sensing*. 2021, 13, 14, 2825. doi: 10.3390/rs13142825
26. *Longuet-Higgins M.S., Stewart R.W.* Changes in the form of short gravity waves on long waves and tidal currents. *Journal of Fluid Mechanics*. 1960, 8, 565–583. doi: 10.1017/S0022112060000803
27. *Phillips O.M.* On the response of short ocean wave components at a fixed wave number to ocean current variations. *Journal of Physical Oceanography*. 1984, 14, 9, 1425–1433. doi: 10.1175/1520–0485(1984)014<1425:OTROSO>2.0.CO;2
28. *Fairall C.W.*, *Bradley E.F.*, *Hare J.E.*, *Grachev A.A.*, *Edson J.B.* Bulk parameterization of air–sea fluxes: Updates and verification for the COARE algorithm. *Journal of Climate*. 2003, 16, 4, 571–591. doi: 10.1175/1520-0442(2003)016<0571: BPOASF>2.0.CO;2
29. *Korinenko A.E.*, *Malinovsky V.V.*, *Kudryavtsev V.N.* Experimental research of statistical characteristics of wind wave breaking. *Physical Oceanography*. 2018, 25, 6, 489–500. doi: 10.22449/1573-160X-2018-6-489-500
30. *Korinenko A.E.*, *Malinovsky V.V.*, *Kudryavtsev V.N.*, *Dulov V.A.* Statistical characteristics of wave breakings and their relation with the wind waves' energy dissipation based on the field measurements. *Physical Oceanography*. 2020, 27, 5, 472–488. doi: 10.22449/1573-160X-2020-5-472-488
31. *Mironov A.S.*, *Dulov V.A.* Detection of wave breaking using sea surface video records. *Measurement Science and Technology*. 2008, 19, 015405. doi: 10.1088/0957-0233/19/1/015405
32. *Kleiss J.M.*, *Melville W.K.* Observations of wave breaking kinematics in fetch-limited seas. *Journal of Physical Oceanography*. 2010, 40, 12, 2575–2604. doi: 10.1175/2010JPO4383.1
33. *Kleiss J.M.*, *Melville W.K.* The analysis of sea surface imagery for whitecap kinematics. *Journal of Atmospheric and Oceanic Technology*. 2011, 28, 2, 219–243. doi: 10.1175/2010JTECHO744.1
34. *Phillips O.M.* Spectral and statistical properties of the equilibrium range in wind-generated gravity waves. *Journal of Fluid Mechanics*. 1985, 156, 505–531. doi: 10.1017/S0022112085002221

Литература

1. *Zappa C.J.*, *McGillis W.R.*, *Raymond P.A.*, *Edson J.B.*, *Hintsa E.J.*, *Zemmelink H.J.*, *Dacey J.W.H.*, *Ho D.T.* Environmental turbulent mixing controls on air-water gas exchange in marine and aquatic systems // Journal of Geophysical Research Letters. 2007. Vol. 34, No 10. doi: 10.1029/2006GL028790

2. *Thorpe S.A.* Energy loss by breaking waves // Journal of Physical Oceanography. 1993. Vol. 23, No 11. P. 2498–2502. doi: 10.1175/1520-0485(1993)023<2498: ELBBW>2.0.CO;2
3. *Kudryavtsev V.N.*, *Shrira V.*, *Dulov V.A.*, *Malinovsky V.V.* On the vertical structure of wind-driven sea currents // Journal of Physical Oceanography. 2008. Vol. 38, No 10. P. 2121–2144. doi: 10.1175/2008JPO3883.1
4. *Troitskaya Y.*, *Kandaurov A.*, *Ermakova O.*, *Kozlov D.*, *Sergeev D.*, *Zilitinkevich S.* Bag-breakup fragmentation as the dominant mechanism of sea-spray production in high winds // Scientific Reports. 2017. Vol. 7. 1614. doi: 10.1038/s41598-017-01673-9
5. *Kudryavtsev V.*, *Chapron B.* On growth rate of wind waves: impact of short-scale breaking modulations // Journal of Physical Oceanography. 2016. Vol. 46, No 1. P. 349–360. doi: 10.1175/JPO-D-14-0216.1
6. *Troitskaya Y.*, *Sergeev D.*, *Kandaurov A.*, *Vdovin M.*, *Zilitinkevich S.* The effect of foam on waves and the aerodynamic roughness of the water surface at high winds // Journal of Physical Oceanography. 2019. Vol. 49. doi: 10.1175/JPO-D-18-0168.1
7. *Thorpe S.A.*, *Belloul M.B.*, *Hall A.J.* Internal waves and whitecaps // Nature. 1987. Vol. 330. P. 740–742. doi: 10.1038/330740a0
8. *Dulov V.A.*, *Kudryavtsev V.N.*, *Sherbak O.G.*, *Grodsky S.A.* Observations of wind wave breaking in the gulf stream frontal zone // The Global Atmosphere and Ocean System. 1998. Vol. 6, No 3. P. 209–242.
9. *Kubryakov A.A.*, *Kudryavtsev V.N.*, *Stanichny S.V.* Application of Landsat imagery for the investigation of wave breaking // Remote Sensing of Environment. 2021. Vol. 253. 112144. doi: 10.1016/j.rse.2020.112144
10. *Бондур В.Г.*, *Шарков Е.А.* Статистические характеристики пенных образований на взволнованной морской поверхности // Океанология. 1982. Т. 22, № 3. С. 372–378.
11. *Monahan E.C.*, *Woolf D.K.* Comments on «Variations of whitecap coverage with wind stress and water temperature» // Journal of Physical Oceanography. 1989. Vol. 19, No 5. P. 706–709. doi: 10.1175/1520-0485(1989)019<0706: COOWCW>2.0.CO;2
12. *Шарков Е.А.* Обрушающиеся морские волны: структура, геометрия, электродинамика. М.: Научный мир, 2009. 304 с.
13. *Phillips O.M.* Radar returns from the sea surface — Bragg scattering and breaking waves // Journal of Physical Oceanography. 1988. Vol. 18, No 8. P. 1065–1074. doi: 10.1175/1520-0485(1988)018<1065: RRFTSS>2.0.CO;2
14. *Kudryavtsev V.N.*, *Hauser D.*, *Caudal G.*, *Chapron B.* A semiempirical model of the normalized radar cross-section of the sea surface 1. Background model // Journal of Geophysical Research. 2003.Vol. 108, No C3. doi: 10.1029/2001JC001003
15. *Шарков Е.А.* Экспериментальные исследования времени жизни дисперсной фазы обрушивающейся гравитационной волны // Известия АН. ФАО. 1994. Т. 30, № 6. С. 844–847.
16. *Callaghan A.H.*, *Deane G.B.*, *Stokes M.D.*, *Ward B.* Observed variation in the decay time of oceanic whitecap foam // Journal of Geophysical Research. 2012. Vol. 117, No C9. doi: 10.1029/2012JC008147
17. *Ding L.*, *Farmer D.M.* Observation of breaking surface wave statistics // Journal of Physical Oceanography. 1994. Vol. 24, No 6. P. 1368–1387. doi: 10.1175/1520-0485(1994)024<1368: OOBSWS>2.0.CO;2
18. *Bortkovskii R.S.*, *Novak V.A.* Statistical dependences of sea state characteristics on water temperature and wind-wave age // Journal of Marine Systems. 1993. Vol. 4, No 2–3. P. 161–169. doi: 10.1016/0924-7963(93)90006-8
19. *Phillips O.M.*, *Posner F.L.*, *Hansen J.P.* High range resolution radar measurements of the speed distribution of breaking events in wind-generated ocean waves: Surface impulse and wave energy dissipation rates // Journal of Physical Oceanography. 2001. Vol. 31, No 2. P. 450–460. doi: 10.1175/1520-0485(2001)031<0450: HRRRMO>2.0.CO;2
20. *Миронов А.С.*, *Дулов В.А.* Статистические характеристики событий и диссипация энергии при обрушении ветровых волн // Сборник научных трудов. Вып. 16. НАН Украины, МГИ, Севастополь, 2008. С. 97–115.
21. *Thorpe S.A.*, *Hall A.J.* The characteristics of breaking waves, bubble clouds, and near-surface currents observed using side-scan sonar // Continental Shelf Research. 1983. Vol. 1, No 4. P. 353–384. doi: 10.1016/0278-4343(83)90003-1
22. *Pivaev P.D.*, *Kudryavtsev V.N.*, *Korinenko A.E.*, *Malinovsky V.V.* Field observations of breaking of dominant surface waves // Remote Sensing. 2021. Vol. 13, No 16. 3321. doi: 10.3390/rs13163321
23. *Dulov V.A.*, *Kudryavtsev V.N.*, *Bol'shakov A.N.* A field study of whitecap coverage and its modulations by energy containing surface waves // Gas Transfer at the Water Surface. Geophys. Monogr. 127 / Ed. Donelan M.A., Drennan W.M., Saltzman E.S., Wanninkhof R. AGU: Washington DC. USA, 2002. P. 187–192. doi: 10.1029/GM127p0187

24. *Yurovsky Y.Y.*, *Kudryavtsev V.N.*, *Chapron B.* Simultaneous radar and video observations of the sea surface in field conditions // Proceedings of the Electromagnetics Research Symposium — Spring (PIERS). St. Petersburg, 2017. P. 2559–2565. doi: 10.1109/PIERS.2017.8262183
25. *Dulov V.A.*, *Korinenko A.E.*, *Kudryavtsev V.N.*, *Malinovsky V.V.* Modulation of wind-wave breaking by long surface waves // Remote Sensing. 2021. Vol. 13, No 14. 2825. doi: 10.3390/rs13142825
26. *Longuet-Higgins M.S.*, *Stewart R.W.* Changes in the form of short gravity waves on long waves and tidal currents // Journal of Fluid Mechanics. 1960. Vol. 8. P. 565–583. doi: 10.1017/S0022112060000803
27. *Phillips O.M.* On the response of short ocean wave components at a fixed wave number to ocean current variations // Journal of Physical Oceanography. 1984. Vol. 14, No 9. P. 1425–1433. doi: 10.1175/1520-0485(1984)014<1425: OTROSO>2.0.CO;2
28. *Fairall C.W.*, *Bradley E.F.*, *Hare J.E.*, *Grachev A.A.*, *Edson J.B.* Bulk parameterization of air–sea fluxes: Updates and verification for the COARE algorithm // Journal of Climate. 2003. Vol. 16, No 4. P. 571–591. doi: 10.1175/1520-0442(2003)016<0571: BPOASF>2.0.CO;2
29. *Кориненко А.Е.*, *Малиновский В.В.*, *Кудрявцев В.Н.* Экспериментальные исследования статистических характеристик обрушений ветровых волн // Морской гидрофизический журнал. 2018. Т. 34, № 6. С. 534–547. doi: 10.22449/0233-7584-2018-6-534-547
30. *Кориненко А.Е.*, *Малиновский В.В.*, *Кудрявцев В.Н.*, *Дулов В.А.* Статистические характеристики обрушений и их связь с диссипацией энергии ветровых волн по данным натурных измерений // Морской гидрофизический журнал. 2020. Т. 36, № 5. С. 514–531. doi: 10.22449/0233-7584-2020-5-514-531
31. *Mironov A.S.*, *Dulov V.A.* Detection of wave breaking using sea surface video records // Measurement Science and Technology. 2008. Vol. 19. P. 015405. doi: 10.1088/0957-0233/19/1/015405
32. *Kleiss J.M.*, *Melville W.K.* Observations of wave breaking kinematics in fetch-limited seas // Journal of Physical Oceanography. 2010. Vol. 40, No 12. P. 2575–2604. doi: 10.1175/2010JPO4383.1
33. *Kleiss J.M.*, *Melville W.K.* The analysis of sea surface imagery for whitecap kinematics // Journal of Atmospheric and Oceanic Technology. 2011. Vol. 28, No 2. P. 219–243. doi: 10.1175/2010JTECHO744.1
34. *Phillips O.M.* Spectral and statistical properties of the equilibrium range in wind-generated gravity waves // Journal of Fluid Mechanics. 1985. Vol. 156. P. 505–531. doi: 10.1017/S0022112085002221